Pd/FeOₓ催化剂动态生成Pdᵟ⁺-Fe²⁺界面高效催化逆水煤气变换反应

张殿宇[1,2]　刘　放[3]　杜鹏飞[1,2]　李梦维[1]　吴兆萱[4]　丰义兵[1]

赵　阳[1]　徐晓燕[1]　张新星[5]　路军岭[3]　杨　冰[*,1]

([1]洁净能源国家实验室,大连化学物理研究所,大连　116023)
([2]中国科学院大学,北京　100049)
([3]中国科学技术大学化学物理系,合肥　230026)
([4]中国科学院,上海高等研究院,上海　201210)
([5]芝加哥大学化学系,芝加哥,美国 IL　60637)

摘要: 通过一系列原位、非原位表征,包括透射电子显微镜(TEM)、傅里叶变换红外光谱(FTIR)、程序升温解吸/还原/氧化(TPD/TPR/TPO)、X射线光电子能谱(XPS)等,系统地研究了Pd/FeOₓ催化剂的逆水煤气变换反应(RWGS)。以Pd(acac)₂为前驱体合成了高度分散的Pd/FeOₓ催化剂,在400 ℃下,RWGS的CO₂转化率高达29%,CO选择性超过98%,在目前文献中报道的催化剂中处于领先水平。通过原位表征方法,我们进一步研究了Pd/SiO₂和Pd-Fe/SiO₂,并明确指出了Pd-FeOₓ界面对促进RWGS反应的重要作用。准原位XPS实验进一步揭示了Pd/FeOₓ界面上动态形成的Pdᵟ⁺-Fe²⁺物种是高效催化C═O离解的活性位点。因此,实验结果证明,反应过程中动态形成的Pdᵟ⁺-Fe²⁺界面可以显著提高RWGS的活性和选择性,对CO₂吸附、C═O解离和CO脱附都起到的促进作用。

关键词: 钯;二氧化碳;界面;反应机理;多相催化

Dynamic Formation of Pdᵟ⁺-Fe²⁺ Interface Promoting Reverse Water Gas Shift Reaction over Pd/FeOₓ Catalyst

ZHANG Dian-Yu[1,2]　LIU Fang[3]　DU Peng-Fei[1,2]　LI Meng-Wei[1]　WU Zhao-Xuan[4]　FENG Yi-Bing[1]
ZHAO Yang[1]　XU Xiao-Yan[1]　ZHANG Xin-Xing[5]　LU Jun-Ling[3]　YANG Bing[*,1]

([1]*Dalian National Laboratory for Clean Energy (DNL), Dalian Institute of Chemical Physics,*
Chinese Academy of Sciences, Dalian, Liaoning 116023, China)
([2]*University of Chinese Academy of Sciences, Beijing 100049, China*)
([3]*Department of Chemical Physics, University of Science and Technology of China, Hefei 230026, China*)
([4]*Shanghai Advanced Research Institute, Chinese Academy of Sciences, Shanghai 201210, China*)
([5]*Department of Chemistry, the University of Chicago, Chicago, IL 60637, United States*)

Abstract: We systematically investigated Pd/FeOₓ for the reverse water gas shift (RWGS) reaction using a combination of *ex situ* and *in situ* characterizations, including transmission electron microscopy (TEM), Fourier-transform infrared (FTIR) spectroscopy, temperature-programmed desorption/reduction/oxidation (TPD/TPR/TPO), and X-ray photoelectron spectroscopy (XPS). A highly dispersed Pd/FeOₓ catalyst was synthesized using Pd(acac)₂ as the precursor. The catalyst exhibited high activity, with CO₂ conversion of ~29% and CO selectivity ogreater than 98% at

400 ℃, which are among the highest values in the literature. Moreover, Pd/SiO$_2$ and Pd-Fe/SiO$_2$ were further studied to determine the significant role of the Pd-FeO$_x$ interface in promoting the RWGS reaction. Semi-*in situ* XPS revealed the dynamic formation of Pd$^{\delta+}$-Fe^{2+} species at the Pd-FeO$_x$ interface; the species acted as highly active sites for CO$_2$ dissociation. Our results also showed the formation of the Pd$^{\delta+}$-Fe^{2+} interface during the RWGS reaction remarkably enhanced the activity and selectivity of the Pd-FeO$_x$ catalyst for the reaction, benefiting CO$_2$ adsorption, C＝O dissociation, and CO desorption.

Keywords: palladium; carbon dioxide; interfaces; reaction mechanisms; heterogeneous catalysis

0　Introduction

　　Carbon dioxide reduction has received tremendous attention for its potential in solving the energy and environmental crises[1-3]. The reverse water gas shift (RWGS) reaction is an effective route for syngas production via CO$_2$ hydrogenation[4-6]. Numerous experimental studies have investigated the RWGS reaction, using Au/MoO$_x$[7], Ru/Al$_2$O$_3$[8], Cu/FeO$_x$[9], and other monometallic[10-12], bimetallic[13], and metal oxides[14] as catalysts. The reaction pathway can be summarized into two theories: the direct path and the indirect path. The direct path involves the direct CO$_2$ dissociation into CO$_{ad}$ and O$_{ad}$, and then the CO$_{ad}$ is desorbed as CO[15]. The indirect path involves the hydrogenation of CO$_2$ via formate or carbonate species as intermediates, and the CO$_2$ further decomposes into CO as the main product[3-4,16-17]. The metal support interface also plays a vital role in the RWGS reaction[6-7,18] and affects the selectivity[9]. To date, the reaction mechanism, including the active interface structure, is still under debate.

　　Iron oxide-supported palladium catalysts have been extensively studied for the RWGS reaction[19], water gas shift (WGS) reaction[20], and CO oxidation[21-23]. The Pd-FeO$_x$ interface has been found to be crucial in a variety of reactions, as it promotes oxygen vacancies and oxygen transportation[24-26]. The higher reducibility of the FeO$_x$-supported Pd species, which feature active interface structures, has also been extensively reported[20,26-28]. However, these works focus solely on the metal-support interaction from a static point of view, determined via *ex situ* characterization[5]. The dynamic evolution of the Pd-FeO$_x$ interface during the reaction has not yet been clarified owing to the lack of *in situ* techniques.

　　In this study, Pd/FeO$_x$, Pd/SiO$_2$, and Pd-Fe/SiO$_2$ catalysts were systematically investigated for the RWGS reaction. The catalytic performance for the RWGS reaction was evaluated, and a promoting role of the Pd-FeO$_x$ interface was observed. Using a combination of *ex situ* and *in situ* characterizations, we identified a dynamic evolution of the Pd-FeO$_x$ interface during reaction, in which interfacial Pd$^{\delta+}$-Fe^{2+} species were formed as the active sites. The underlying reaction mechanism and the role of the Pd-FeO$_x$ interface were further investigated using temperature-programmed desorption/reduction/oxidation (TPD/TPR/TPO) and Fourier-transform infrared (FTIR) spectroscopy.

1　Experimental

1.1　Catalysts preparation

　　The FeO$_x$ sample was prepared by the precipitation of Fe(NO$_3$)$_3$·9H$_2$O in a NaOH solution. The Pd/FeO$_x$ catalyst was prepared by the impregnation method, with 28.8 mg Pd(acac)$_2$ as the precursor and 200 mg FeO$_x$ and 60 mL toluene as the solvent in a flask[29]. Moreover, Pd/SiO$_2$ was prepared by a wet impregnation method, using 148.5 mg Pd(NH$_3$)$_4$Cl$_2$·H$_2$O and 1 g SiO$_2$. A GEMSTAR-6TM Benchtop atomic layer deposition (ALD) system was used to synthesize Pd-Fe/SiO$_2$[30]. Nitrogen (99.999%) was the carrier gas at 200 mL·min^{-1}, and FeO$_x$ ALD was performed at 150 ℃ by exposing the as-prepared Pd/SiO$_2$ to 20~25 cycles of ferrocene and oxygen (For more details, see in Supplementary Information).

1.2　Catalytic testing

　　Catalytic testing was performed in a continuous-flow fixed-bed reactor with 40 mg of catalyst under

atmospheric pressure, with a feed gas of 24% CO_2 and 72% H_2 (volume fraction, unless otherwise specified, all other gas contents in the paper are volume fractions), balanced with Ar. The total flow was 24 mL·min^{-1}, which resulted in a weight hourly space velocity of 36 000 mL·h^{-1}·g$_{cat}$$^{-1}$. After the gas phase was allowed to stabilize for 30 min to reach the steady-state for each reaction temperature, the outlet gas composition was analyzed by an on-line gas chromatograph (Agilent 7820A) equipped with a thermal conductivity detector and a flame ionization detector, and He was the carrier gas.

CO_2 conversion was calculated as follows:

$$X_{CO_2} = \frac{n_0 - n_1}{n_0} \times 100\% \tag{1}$$

Where n_0 and n_1 stand for the amounts of CO_2 in feed gas and outlet gas.

CO selectivity was calculated as follows:

$$S_{CO} = \frac{n_{CO}}{n_0 - n_1} \times 100\% \tag{2}$$

Where n_{CO} stands for the amount of CO in outlet gas.

1.3 Catalysts characterization

X-ray diffraction (XRD, PAN analytical, X′ Pert PRO X) was performed with a Cu $K\alpha$ radiation source (λ =0.154 06 nm) in reflection mode. X-ray tube was operated at 40 kV and 40 mA. XRD diffraction range was set to 15° to 85°.

The catalysts were characterized via high-resolution transmission electron microscopy (TEM), using a JEOL JEM-2100 microscope at 200 kV. The sample was dispersed by ethanol under ultrasonication. The samples were also analyzed via energy-dispersive X-ray spectroscopy (EDS), using the Aztec X-Max 80T EDS system (Oxford instrument, UK).

Hydrogen temperature-programmed reduction (TPR) was performed on a Micromeritics AutoChem Ⅱ chemisorption analyzer. First, 50 mg catalyst was loaded into a U-shape quartz reactor and purged with helium at 120 ℃ for 2 h to remove physically adsorbed water and surface carbonates. After the catalyst was cooled to −50 ℃, the gas was switched to a flow of 10% (V/V) H_2 balanced with Ar, and the catalyst was heated to 500 ℃ at a ramping rate of 10 ℃·min^{-1}. The amount

of H_2 consumption was calculated with the H_2 peak area and calibration curve of the 10% (V/V) H_2 balanced with Ar standard gas.

Furthermore, CO_2 temperature-programmed desorption (TPD) experiments were performed on the AutoChem Ⅱ 2920. The samples were placed in a quartz tube. Before the TPD experiment, all of the samples were pre-reduced by 10% (V/V) H_2/Ar at 300 ℃ for 30 min and then cooled down to room temperature (RT). Then the gas was switched to 10% (V/V) CO_2/Ar at 50 mL·min^{-1} for 1 h for the saturated adsorption of CO_2. After N_2 was purged for 30 min, the sample was heated from 50 to 800 ℃ at a ramping rate of 10 ℃·min^{-1}, during which TPD data were obtained.

Cyclic H_2-TPR and CO_2 temperature-programmed oxidation (TPO) experiments were performed on an OmniSTAR gas analysis system. First, 20 mg catalyst was loaded into a U-shape quartz reactor and purged with helium at 150 ℃ for 2 h to remove physically adsorbed water and surface carbonates. After the temperature was cooled to room temperature, the gas was switched to a flow of 5% (V/V) H_2 balanced with He, and the catalyst was heated to 400 ℃ at a ramping rate of 10 ℃·min^{-1}. Before the CO_2-TPO experiment, the sample was purged again with He at 150 ℃ for 2 h. After the temperature was cooled to room temperature, the gas was switched to a flow of 5% (V/V) CO_2 balanced with He, and the catalyst was heated to 400 ℃ at a ramping rate of 10 ℃·min^{-1}.

The FTIR spectra of CO adsorption were recorded in transmission mode on a Bruker Tensor 27 model. CO was introduced for 30 min at room temperature to reach saturated adsorption, followed by purging with N_2 to remove gaseous CO.

X-ray photoelectron spectroscopy (XPS) experiments were performed using ThermoFisher ESCALAB 250Xi. A semi-*in situ* experiment was conducted by transferring the catalyst directly for XPS measurements after a certain treatment without exposing the catalyst to air, as reported elsewhere[31]. The first set of experiments consisted of a reaction gas (24% CO_2+72% H_2+4% Ar, V/V) treatment for 30 min at room temperature and 400 ℃. The second set of experiments included

three steps for each catalyst. First, the as-prepared catalyst was purged with N$_2$ at room temperature. Then, the sample was heated to 400 ℃ under 10% (V/V) H$_2$/Ar for 30 min. Finally, the gas was switched to 10% (V/V) CO$_2$/Ar for 30 min. The sample was transferred back to the analysis chamber for XPS measurements in between each treatment.

2　Results and discussion

2.1　Catalysts characterization

The TEM images of as-prepared Pd-Fe/SiO$_2$ and the Pd/FeO$_x$ catalysts are displayed in Fig.1a and 1b. The Pd-Fe/SiO$_2$ showed uniformly dispersed Pd nanoparticles (NPs) of ~3 nm on amorphous SiO$_2$. In contrast, Pd/FeO$_x$ displayed a highly polycrystalline FeO$_x$, with no significant Pd particle present (see EDS mapping in Fig.S1). The EDS spectra identified the presence of Pd with a similar loading (Table S1) measured by inductively coupled plasma-optical emission spectrometry (Table S2). The results indicate that a system of highly dispersed Pd species, with a size likely below 2 nm, in as-prepared 3.6% (mass fraction) Pd/FeO$_x$ catalysts was formed[32-33].

Fresh (as-prepared) and spent catalysts were examined via XRD, and the results are presented in Fig.1c. The fresh FeO$_x$ and the 3.6% (mass fraction) Pd/FeO$_x$ catalysts before reaction showed a typical XRD pattern of Fe$_2$O$_3$, which was reduced to Fe$_3$O$_4$ completely after the RWGS reaction. The absence of Pd and PdO XRD patterns in both the fresh and spent Pd/FeO$_x$ catalyst indicates the presence of small Pd/PdO$_x$ nanoparticles (<2 nm) or amorphous nature of Pd species in accordance with the TEM results[34]. In the XRD patterns of the Pd/SiO$_2$ and Pd-Fe/SiO$_2$, a broad band existed at 21.9°, which can be assigned to amorphous SiO$_2$. The additional diffraction peaks at 40.4°, 46.7°, and 68.4° are ascribed to Pd NPs. Moreover, no FeO$_x$ or Fe diffraction peaks were observed in Pd-Fe/SiO$_2$, suggesting a very thin layer of Fe species on the ALD-synthesized Pd NPs.

In the H$_2$-TPR results (Fig.1d), the blank FeO$_x$ support showed two reduction peaks: at 280 and 390 ℃, which are characteristic of the reduction of Fe$_2$O$_3$ to Fe$_3$O$_4$[20]. In the case of the Pd/FeO$_x$ catalyst, the first peak (0 ℃) is ascribed to the reduction of PdO, and the latter two (150 and 250 ℃) are associated with the reduction of FeO$_x$, which shift to lower temperatures. The presence of Pd thus facilitates the reduction of FeO$_x$, likely via H$_2$ spillover effect[20,24]. Compared with the H$_2$-TPR results of Pd/SiO$_2$ and Pd-Fe/SiO$_2$, the significantly enhanced H$_2$ consumption of Pd/FeO$_x$ at 0 ℃ indicates a promoted reduction of the Pd-FeO$_x$ interface, since the H$_2$ consumption was far more than the stoichiometric PdO amount (Table S3 and supple-
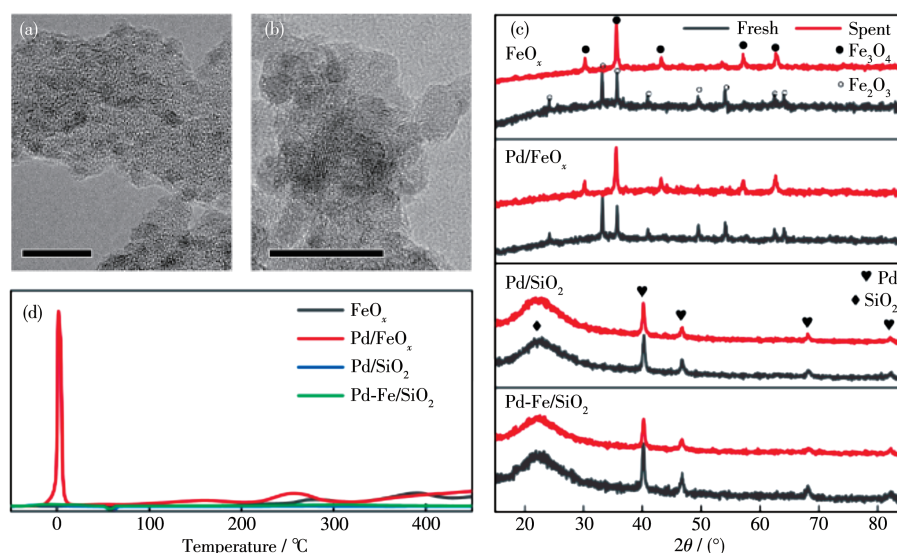

Fig.1　TEM images of Pd-Fe/SiO$_2$ (a) and Pd/FeO$_x$ (b), inserted scale bar is 10 nm; (c) XRD patterns of the fresh and spent catalysts; (d) H$_2$-TPR results of Pd/FeO$_x$, blank FeO$_x$, Pd/SiO$_2$, and Pd-Fe/SiO$_2$ catalysts

mentary discussion). In addition, Pd-Fe/SiO$_2$ also showed a small reduction peak at 320 ℃, which corresponds to the reduction of ALD-synthesized FeO$_x$ on Pd NPs.

2.2　Catalytic tests

The catalytic test was performed in a fixed-bed reactor under atmospheric pressure, with a feed gas of 24% CO$_2$ and 72% H$_2$ (V/V), balanced with Ar. As shown in Fig.2a and 2b, the Pd/FeO$_x$ catalyst exhibited a remarkably high activity for the RWGS reaction, with a CO$_2$ conversion of 10% at 300 ℃ and 29% at 400 ℃, and a CO selectivity of over 98% at all reaction temperatures. In contrast, both the blank FeO$_x$ and Pd/SiO$_2$ catalysts were inactive, with CO$_2$ conversion below 5% at temperatures up to 400 ℃ (see carbon balance data in Table S4). This strongly indicates that the Pd-FeO$_x$ interface is highly required for the RWGS reaction. To further prove this point, a thin layer of FeO$_x$ (mass fraction of 1.1%) was added onto the inactive Pd/SiO$_2$ using ALD (the formed product was denoted as Pd-Fe/SiO$_2$ catalyst). The Pd-Fe/SiO$_2$ catalyst showed a dra-

matically enhanced CO$_2$ conversion, from 5% to 20%, at 400 ℃ (Fig.2c). Only a slight deactivation (<4%) was observed, which was likely due to coking or mild sintering (Fig.S2 and S3). The enhanced activities of Pd/FeO$_x$ and Pd-Fe/SiO$_2$ compared with those of their counterparts (FeO$_x$ and Pd/SiO$_2$) reveal the promoting role of the Pd-FeO$_x$ interface as highly active sites for catalytic CO$_2$ hydrogenation. The long-term stability test of the Pd/FeO$_x$ catalyst was performed at 400 ℃ with time on stream up to 30 h, as shown in Fig.2d. The CO$_2$ conversion and CO selectivity remain stable at ~29% and ~98% over the entire testing, suggesting an excellent stability of the catalyst. The water formation during reaction also shows a minor effect on the catalytic performance of Pd/FeO$_x$ catalyst, with no significant deactivation in both CO$_2$ conversion and CO selectivity (Fig.S4).

Furthermore, the Pd-FeO$_x$ interface also promoted CO selectivity. As shown in Fig.2b, the CO selectivity on the Pd/SiO$_2$ catalyst declined with increasing reaction temperature. The production of methane thus sug-
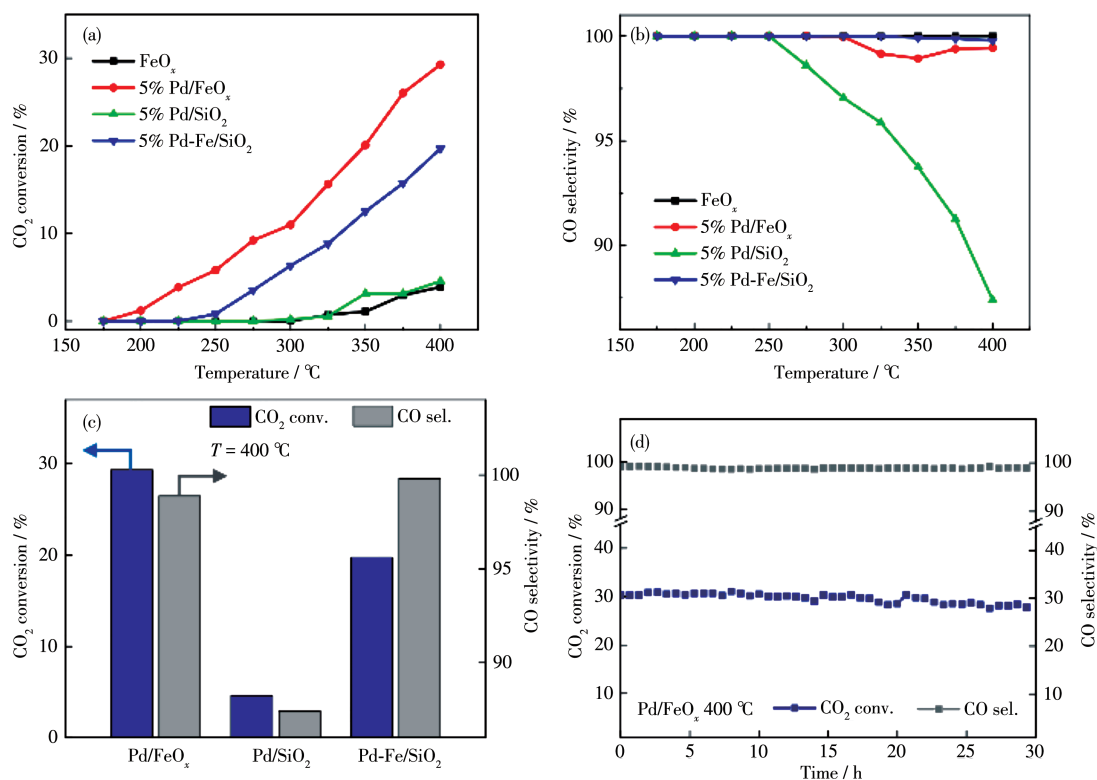

Fig.2　Catalytic performance of all of the catalysts tested for RWGS: (a) CO$_2$ conversion; (b) CO selectivity; (c) Comparison of Pd/FeO$_x$, Pd /SiO$_2$, and Pd-Fe/SiO$_2$ at 400 ℃; (d) Long term stability of Pd/FeO$_x$ catalyst at 400 ℃ with time on stream up to 30 h

gests a deep hydrogenation of CO on Pd/SiO_2 at elevated temperatures. In comparison, both Pd/FeO_x and Pd-Fe/SiO$_2$ catalysts maintained a CO selectivity of over 98% at all temperatures, suggesting that the addition of FeO_x could prevent the further hydrogenation of CO to methane. Table 1 summarizes the catalytic performance of other literature-reported RWGS catalysts.

The 3.6% (mass fraction) Pd/FeO_x and 4.4% (mass fraction) Pd-Fe/SiO$_2$ catalysts in this work features a higher activity and CO selectivity than 1.5% (mass fraction) Rh/SrTiO$_3$[35], 1.67% (mass fraction) Pt/TiO_2[10], 3% (mass fraction) Pd/Fe_3O_4[19], and other metal carbide catalysts[13,36].

Table 1　Summary of the conditions and reactivities of various catalysts in this work and the literature

Catalyst[a]	V_{H_2}/V_{CO_2}	T / ℃	Weight hourly space velocity / (L·h⁻¹·g⁻¹)	X_{CO_2} / %	S_{CO} / %
3.6% Pd/FeO_x (this work)	3	300	36	11	100
4.4% Pd-Fe/SiO$_2$ (this work)	3	300	36	6	100
3.6% Pd/FeO_x (this work)	3	400	36	29	100
4.4% Pd-Fe/SiO$_2$ (this work)	3	400	36	20	100
Mo_2C[36]	3	300	36	8.7	93.9
7.5% Co/Mo_2C[36]	3	300	36	9.5	99
1.67% Pt/TiO_2[10]	1	300	351	4.5	99.1
1.67% Pt/SiO_2[10]	1	300	72.1	3.3	100
1.1% Rh/SrTiO$_3$[35]	1	300	120	7.9	95.4
5% Co/MCF-17[13]	3	200~300	60	~5	90
5% Pt50Co50/MCF-17[13]	3	200~300	60	~5	99
1% Pt/TiO_2[11]	3	600	12	~58	~95
3% Pd/Fe_3O_4 (dopPPh$_2$)[19]	4	400	60	8.8	94.6

[a] All the percents are mass fraction.

2.3　Dynamic formation of Pd^δ⁺-Fe²⁺ interface as determined by *semi-in situ* XPS

To identify the dynamic evolution of surface active sites, semi-*in situ* XPS experiments were performed, which enabled transferring the catalyst directly for XPS measurements after certain treatment without exposing it to air (for details, see in supplementary methods). The Pd/FeO_x, Pd/SiO_2, and Pd-Fe/SiO$_2$ catalysts were stepwise heated in 10% H$_2$ and 10% CO$_2$ at 400 ℃, and the Pd3d core-level evolution spectra are displayed in Fig.3a. Three characteristic chemical states of Pd species could be identified from the evolution spectra: 337.2 eV[37], for oxidized Pd²⁺ state; 335.7 eV[38], for partially oxidized Pd^δ⁺ state; and 334.8 eV[38], for metallic Pd⁰ state (Fig.S5~S8). For Pd/SiO_2, the pristine catalyst showed a Pd3$d_{5/2}$ binding energy (BE) of 355.6 eV, corresponding to a Pd^δ⁺ state, which likely originated from the native oxide on the Pd NPs. In previous studies, a similar Pd^δ⁺ state was revealed by

ambient-pressure XPS as a surface oxide and further assigned to Pd$_5$O$_4$ stoichiometry[39-41]. Reduction in H$_2$ at 400 ℃ led to a prominent metallic Pd⁰ of 334.8 eV, which re-oxidized to a Pd^δ⁺ state in the subsequent CO$_2$ treatment (400 ℃). Considering the chemical inertness of the SiO_2 support, we can conclude that Pd⁰ was oxidized to Pd^δ⁺ by CO$_2$ at 400 ℃, strongly indicating a direct dissociation of CO$_2$ to CO on Pd NPs. The pristine Pd-Fe/SiO$_2$ and Pd/FeO_x catalysts showed a higher Pd3$d_{5/2}$ BE of 336.8 and 337.2 eV respectively, characteristic of PdO oxides[37]. The similar redox properties of Pd-Fe/SiO$_2$ and Pd/FeO_x under H$_2$ and CO$_2$ treatments indicate the same reaction path of direct CO$_2$ dissociation for the RWGS reaction. Moreover, the addition of FeO_x significantly promoted the enrichment of Pd^δ⁺ species in the reduced Pd/SiO_2, Pd-Fe/SiO$_2$, and Pd/FeO_x catalysts after H$_2$ treatment, as indicated by the gradual upshift of Pd3$d_{5/2}$ BE from metallic Pd⁰ to Pd^δ⁺ (334.8, 335.0, and 335.7 eV for Pd/SiO_2, Pd-Fe/

SiO_2, and Pd/FeO_x, respectively) with increasing FeO_x content. The formation of $Pd^{\delta+}$ species during the RWGS reaction was further verified by the treatment of Pd/FeO_x, Pd/SiO_2, and Pd‐Fe/SiO$_2$ catalysts under the reaction gas of 24% CO_2+72% H_2+4% Ar (V/V) at 400 ℃. As shown in Fig.3b, Fig.S9, and Table S5, the Pd/FeO_x, Pd/SiO_2, and $Pd-Fe/SiO_2$ catalysts after reaction exhibited a prominent $Pd^{\delta+}$ state with a $Pd3d_{5/2}$ peak of 335.7 eV, which further indicates the stability of the $Pd^{\delta+}$ surface oxides during the RWGS reaction.

The Fe2p XPS core‐level spectra are displayed in Fig.3c and Fig.S10~S11. In the stepwise H_2/CO_2 heating experiments (Fig.3c), an evolution of the chemical state of iron oxides in $Pd-Fe/SiO_2$ occurred, resulting in a downshift of Fe2$p_{3/2}$ BE from 711.0 eV (Fe^{3+} state) to 710.3 eV (a reduced Fe^{2+} state) after H_2 reduction and an upshift back to 711.0 eV after CO_2 treatment. The dynamic formation of Fe^{2+} species was thus facilitated by H_2 reduction, and the Fe^{2+} species were further re‐oxidized to Fe^{3+} state by reacting with CO_2. A similar oscillation of the Fe2$p_{3/2}$ core level was also observed on Pd/FeO_x, but less prominent owing to the higher
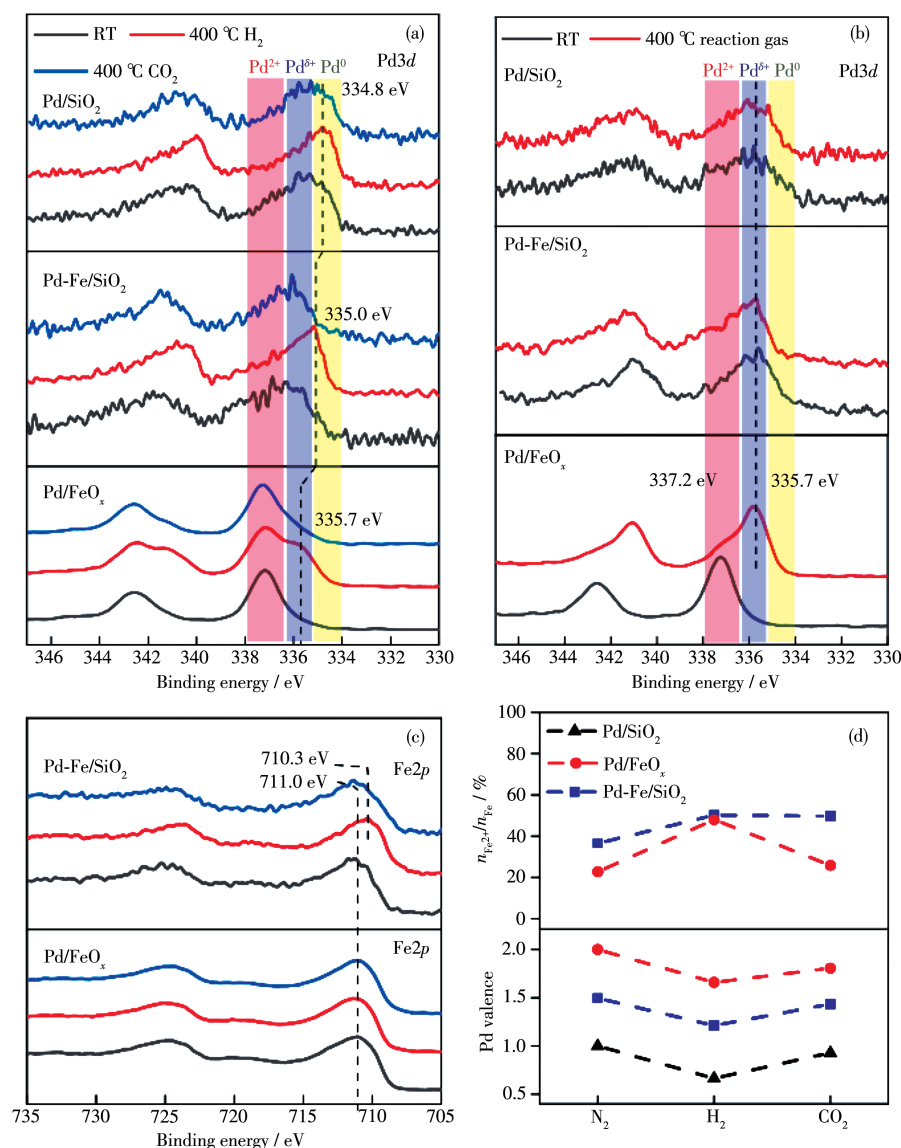

Fig.3 *Semi-in situ* XPS spectra: Pd3d core-level spectra of Pd/FeO_x, Pd/SiO_2, and $Pd-Fe/SiO_2$ catalysts during stepwise H_2 and CO_2 treatments (a) and after 400 ℃ treatment in the reaction gas (b); (c) Fe2p core-level spectra of Pd/FeO_x, Pd/SiO_2, and $Pd-Fe/SiO_2$ catalysts during stepwise H_2 and CO_2 treatments; (d) Oscillation of Fe^{2+} concentration and Pd valence state, deduced from Fe2p and Pd3d XPS results

background signal from the bulk Fe_2O_3 support in the Pd/FeO$_x$ catalyst. This further indicates the surface-enrichment of Fe^{2+} species on the Pd/FeO$_x$ catalyst, formed via hydrogen spillover to the periphery of the Pd NPs[42-43]. After reaction gas treatment (Fig.S12), the Fe2$p_{3/2}$ of both Pd/FeO$_x$ and Pd-Fe/SiO$_2$ underwent a downshift from 710.9 to 710.4 eV, and the characteristic satellite peak for Fe_2O_3 (718 eV) was absent[44], suggesting a reduction in iron oxide support, which agrees with our XRD results. Further reduction of the surface/bulk Fe species may require higher temperature or extended reaction time.

Fig.3d displays the oscillation of Fe^{2+} concentration and Pd valence state deduced from Fe2p and Pd3d XPS results, as summarized in Tables S6 and S7. The enrichment of Pd$^{\delta+}$-Fe^{2+} on both Pd-Fe/SiO$_2$ and Pd/FeO$_x$ was identified under dynamic reduction by H_2, so that the Pd$^{\delta+}$-Fe^{2+} further transformed into Pd^{2+}-Fe^{3+} after reacting with CO_2. Based on the higher activities of Pd-Fe/SiO$_2$ and Pd/FeO$_x$ compared with that of Pd/SiO$_2$, we can assign the dynamic Pd$^{\delta+}$-Fe^{2+} interface as a highly active site for CO_2 dissociation during RWGS.

2.4 Promoting role of Pd-FeO$_x$ interface in adsorption/desorption process

Fig.4a displays the FTIR spectra of CO adsorption over spent catalysts. Two vibrational bands of CO stretching modes, at 2 086 and 1 965 cm^{-1}, were observed on Pd/SiO$_2$, which can be assigned to CO adsorption on multi-coordinated sites of Pd NPs[45-46]. Moreover, the CO adsorption intensity dramatically diminished on Pd-Fe/SiO$_2$ and eventually became invisible on Pd/FeO$_x$. The absence of CO adsorption on Pd/FeO$_x$ can be ascribed to the higher oxidized Pd$^{\delta+}$/Pd^{2+} state, which may also lead to encapsulation via strong metal-support interaction[47]. The weakening of CO adsorption promoted by iron oxides facilitated the desorption of CO as a product and prevented the deep hydrogenation for methane formation.

Fig.4b presents the CO_2-TPD spectra of reduced FeO$_x$, Pd/SiO$_2$, Pd/FeO$_x$, and Pd-Fe/SiO$_2$ at temperatures up to 750 ℃. All of the tested catalysts were pre-reduced in 10% H_2 at 300 ℃. FeO$_x$ presented only a subtle peak at 400 ℃, suggesting a very weak CO_2 adsorption on Fe_2O_3. In contrast, Pd/SiO$_2$ showed a desorption peak at ~550 ℃, which can be ascribed to the molecular/reactive desorption of chemically adsorbed CO_2 on Pd NPs in a mixed Pd^0/Pd$^{\delta+}$ state, as identified by XPS. An additional desorption peak at higher temperatures (~670 ℃) was observed on both Pd/FeO$_x$ and Pd-Fe/SiO$_2$, reflecting an enhanced CO_2 adsorption owing to the Pd$^{\delta+}$-FeO$_x$ interface, which will lead to the formation of carbonate species or other adsorbed intermediates[48].
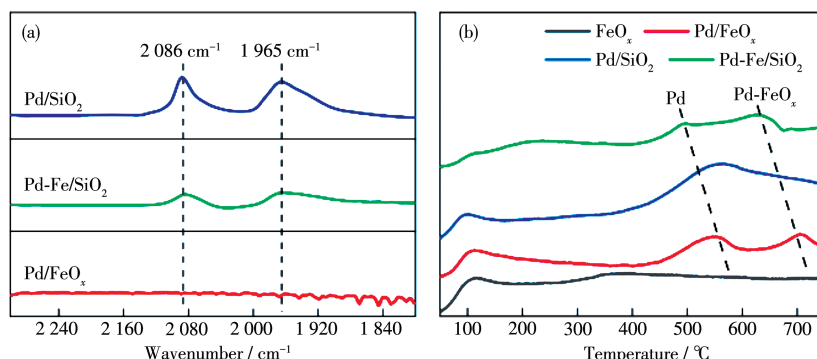

Fig.4　CO and CO_2 adsorption: (a) FTIR spectra of CO adsorption over spent Pd/SiO$_2$, Pd-Fe/SiO$_2$, and Pd/FeO$_x$ catalysts (All IR spectra were acquired at room temperature after evacuating gaseous CO); (b) CO_2-TPD spectra of reduced FeO$_x$, Pd/SiO$_2$, Pd/FeO$_x$, and Pd-Fe/SiO$_2$ at temperatures up to 750 ℃

2.5 Reaction mechanism

The semi-*in situ* XPS results demonstrated a dynamic evolution of Pd and Fe chemical states. To further reveal the reaction pathway, we performed cyclic H_2-TPR and CO_2-TPO on Pd/SiO$_2$ and Pd/FeO$_x$ catalysts. In the case of the Pd/SiO$_2$ catalyst (Fig. 5a), an
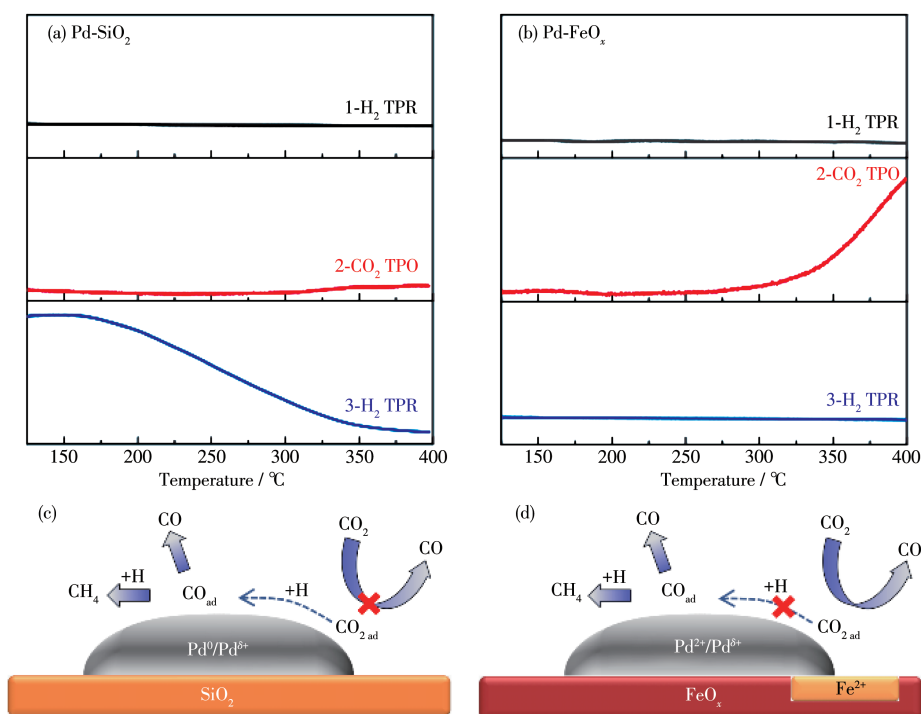
Fig.5　Cyclic H_2-TPR/CO_2-TPO experiments on Pd/SiO_2 (a) and Pd/FeO_x (b) catalysts (Y-axis is the ion intensity of m/z=28 for CO); Schematic reaction path of CO_2 hydrogenation on Pd/SiO_2 (c) and Pd/FeO_x (d) catalysts
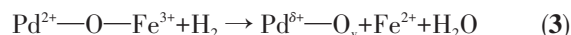
indirect path was identified, as indicated by the pronounced CO production along the second H_2-TPR cycle, via the hydrogenation of either adsorbed CO_2 or carbonate species on the metallic Pd surfaces[17,49]. Meanwhile, the formation of a little amount of CO was also detected in the CO_2-TPO cycle, suggesting the coexistence of direct CO_2 dissociation, likely on the remanence of $Pd^{\delta+}$ species, as identified in the semi-*in situ* XPS experiments. Moreover, the Pd/FeO_x (Fig.5b) showed a remarkably enhanced CO formation in the CO_2-TPO cycle (direct path), while the hydrogenation path (indirect path) was significantly inhibited, as no CO signal was observed in the second H_2-TPR cycle.

Based on the dynamic evolution of the Pd/Fe chemical state based on the semi-*in situ* XPS results, we can propose the overall reaction pathways and underlying mechanism for the RWGS reaction over Pd-Fe catalysts (Fig.5c and 5d).

(1) On Pd/SiO_2, the majority of CO_2 is hydrogenated on the metallic Pd surface via an indirect path, leading to the formation of formate or bicarbonate intermediates, which are eventually decomposed to produce CO. Though less favorable, the direct path of CO_2 disso-

ciation also coexists on Pd/SiO_2, which is likely facilitated by the remanence of $Pd^{\delta+}$ species near the SiO_2 interface. The enhanced CO adsorption on metallic Pd^0 favors the deep hydrogenation of CO, leading to undesired CH_4 as a byproduct[50]. The low activity of Pd/SiO_2 is caused by the weak CO_2 adsorption, as indicated by the CO_2-TPD experiments.

(2) On Pd/FeO_x and Pd-Fe/SiO_2, the Pd-FeO_x interface significantly enhances the CO_2 adsorption, resulting in a remarkably high CO_2 conversion compared with that on Pd/SiO_2. The dynamic formation of $Pd^{\delta+}$-Fe^{2+} species promoted CO_2 dissociation, likely following the Mars-van Krevelen mechanism, via active oxygen vacancies on the interface[8,18,43]:

$$Pd^{2+}—O—Fe^{3+}+H_2 \rightarrow Pd^{\delta+}—O_v+Fe^{2+}+H_2O \quad (3)$$
$$Pd^{\delta+}—O_v+Fe^{2+}+CO_2 \rightarrow Pd^{2+}—O\text{-}Fe^{3+}+CO \quad (4)$$

The weakening of CO adsorption on the oxidized $Pd^{\delta+}$/Pd^{2+} species enriched by iron oxide further enhances the CO selectivity (>98%) by preventing the deep hydrogenation for CH_4 formation.

3　Conclusions

In this study, Pd/FeO_x, Pd-Fe/SiO_2, Pd/SiO_2, and

FeO$_x$ catalysts were systematically investigated for the RWGS reaction. The Pd/FeO$_x$ and Pd-Fe/SiO$_2$ catalysts exhibited extraordinary activity for the RWGS reaction, with CO$_2$ conversions of 29% and 20% at 400 ℃, respectively, and remarkably high CO selectivity (over 98%) at all considered reaction temperatures. Thus, the Pd-FeO$_x$ interface promoted the CO$_2$ hydrogenation to CO. Moreover, semi-*in situ* XPS and cyclic TPR/TPO experiments identified the dynamic formation of Pd$^{\delta+}$-Fe^{2+} species during the RWGS reaction; the species acted as highly active sites for direct CO$_2$ dissociation via oxygen vacancies enriched on the interface. The formation of Pd$^{\delta+}$-FeO$_x$ species was confirmed to play a significant role in the CO$_2$ adsorption and CO desorption, as they further enhanced the catalytic activity and selectivity of CO for the RWGS reaction. Our results provide new insights for the dynamic understanding of the metal-oxide interfaces during reactions and benefit the rational design of heterogeneous catalysts from a dynamic point of view.

Supporting information is available at http://www.wjhxxb.cn

References:

[1] Li W H, Wang H Z, Jiang X, Zhu J, Liu Z M, Guo X W, Song C S. *RSC Adv.*, **2018**,**8**(14):7651-7669

[2] Dorner R W, Hardy D R, Williams F W, Willauer H D. *Energy Environ. Sci.*, **2010**,**3**(7):884-890

[3] Wang W, Wang S P, Ma X B, Gong J L. *Chem. Soc. Rev.*, **2011**,**40**(7): 3703-3727

[4] Daza Y A, Kuhn J N. *RSC Adv.*, **2016**,**6**(55):49675-49691

[5] Parkinson G S. *Surf. Sci. Rep.*, **2016**,**71**(1):272-365

[6] Liu M, Yi Y H, Wang L, Guo H C, Bogaerts A. *Catalysts*, **2019**,**9**(3): 275

[7] Carrasquillo-Flores R, Ro I, Kumbhalkar M D, Burt S, Carrero C A, Alba-Rubio A C, Miller J T, Hermans I, Huber G W, Dumesic J A. *J. Am. Chem. Soc.*, **2015**,**137**(32):10317-10325

[8] Yan Y, Wang Q J, Jiang C Y, Yao Y, Lu D, Zheng J W, Dai Y H, Wang H M, Yang Y H. *J. Catal.*, **2018**,**367**:194-205

[9] Halder A, Kilianová M, Yang B, Tyo E C, Seifert S, Prucek R, Panáček A, Suchomel P, Tomanec O, Gosztola D J, Milde D, Wang H H, Kvítek L, Zbořil R, Vajda S. *Appl. Catal. B*, **2018**,**225**:128-138

[10]Kattel S, Yan B H, Chen J G, Liu P. *J. Catal.*, **2016**,**343**:115-126

[11]Kim S S, Park K H, Hong S C. *Fuel Process. Technol.*, **2013**,**108**:47-54

[12]Chen Y, Lin J, Li L, Qiao B T, Liu J Y, Su Y, Wang X D. *ACS Catal.*, **2018**,**8**(2):859-868

[13]Alayoglu S, Beaumont S K, Zheng F, Pushkarev V V, Zheng H M, Iablokov V, Liu Z, Guo J H, Kruse N, Somorjai G A. *Top. Catal.*, **2011**,**54**(13/14/15):778-785

[14]Zhang Y L, Fu D L, Liu X L, Zhang Z P, Zhang C, Shi B F, Xu J, Han Y F. *ChemCatChem*, **2018**,**10**(6):1272-1276

[15]Fujita S. *J. Catal.*, **1992**,**134**(1):220-225

[16]Goguet A, Meunier F C, Tibiletti D, Breen J P, Burch R. *J. Phys. Chem. B*, **2004**,**108**(52):20240-20246

[17]Boccuzzi F, Chiorino A, Manzoli M, Andreeva D, Tabakova T. *J. Catal.*, **1999**,**188**(1):176-185

[18]Bobadilla L F, Santos J L, Ivanova S, Odriozola J A, Urakawa A. *ACS Catal.*, **2018**,**8**(8):7455-7467

[19]Caparrós F J, Soler L, Rossell M D, Angurell I, Piccolo L, Rossell O, Llorca J. *ChemCatChem*, **2018**,**10**(11):2365-2369

[20]Sun X C, Lin J, Zhou Y L, Li L, Su Y, Wang X D, Zhang T. *AlChE J.*, **2017**,**63**(9):4022-4031

[21]Pavlova S N, Savchenko V I, Sadykov V A, Zaikovskii V I, Kalinkin A V. *React. Kinet. Catal. Lett.*, **1996**,**59**(1):103-110

[22]Bi Y S, Dang G Y, Zhao X H, Meng X F, Lu H J, Jin J T. *J. Hazard. Mater.*, **2012**,**229-230**:245-250

[23]Liu L Q, Zhou F, Wang L G, Qi X J, Shi F, Deng Y Q. *J. Catal.*, **2010**,**274**(1):1-10

[24]Hensley A J R, Hong Y C, Zhang R Q, Zhang H, Sun J M, Wang Y, McEwen J S. *ACS Catal.*, **2014**,**4**(10):3381-3392

[25]Cheng Z, Qin L, Guo M, Fan J A, Xu D, Fan L S. *Phys. Chem. Chem. Phys.*, **2016**,**18**(24):16423-16435

[26]Liang J X, Yu Q, Yang X F, Zhang T, Li J. *Nano Res.*, **2018**,**11**(3): 1599-1611

[27]Fu Q, Li W X, Yao Y, Liu H, Su H Y, Ma D, Gu X K, Chen L, Wang Z, Zhang H, Wang B, Bao X. *Science*, **2010**,**328**(5982):1141-1144

[28]Sun Y N, Giordano L, Goniakowski J, Lewandowski M, Qin Z H, Noguera C, Shaikhutdinov S, Pacchioni G, Freund H J. *Angew. Chem. Int. Ed.*, **2010**,**49**(26):4418-4421

[29]Xie Y H, Li B, Weng W Z, Zheng Y P, Zhu K T, Zhang N W, Huang C J, Wan H L. *Appl. Catal. A*, **2015**,**504**:179-186

[30]Yi H, Xia Y J, Yan H, Lu J L. *Chin. J. Catal.*, **2017**,**38**(9):1581-1587

[31]Hong Y C, Zhang H, Sun J M, Ayman K M, Hensley A J R, Gu M, Engelhard M H, McEwen J S, Wang Y. *ACS Catal.*, **2014**,**4**(10):3335-3345

[32]Sun W Z, Li Q, Gao S A, Shang J K. *Appl. Catal. B*, **2012**,**125**:1-9

[33]Jiang T, Du S C, Jafari T, Zhong W, Sun Y, Song W Q, Luo Z, Hines W A, Suib S L. *Appl. Catal. A*, **2015**,**502**:105-113

[34]Wang F G, Xu Y, Zhao K F, He D N. *Nano-micro Lett.*, **2014**,**6**(3): 233-241

[35]Yan B H, Wu Q Y, Cen J J, Timoshenko J, Frenkel A I, Su D, Chen X Y, Parise J B, Stach E, Orlov A, Chen J G. *Appl. Catal. B*, **2018**, **237**:1003-1011

[36]Porosoff M D, Yang X F, Boscoboinik J A, Chen J G. *Angew. Chem. Int. Ed.*, **2014**,**53**(26):6705-6709

[37]Brun M, Berthet A, Bertolini J C. *J. Electron. Spectrosc. Relat. Phenom.*,

1999,104(1/2/3):55-60

[38]Tura J M, Regull P, Victori L S, de Castellar M D. *Surf. Interface Anal.*, **1988,11**(8):447-449

[39]Klikovits J, Napetschnig E, Schmid M, Seriani N, Dubay O, Kresse G, Varga P. *Phys. Rev. B*, **2007,76**(4):045405

[40]Duan Z Y, Henkelman G. *ACS Catal.*, **2014,4**(10):3435-3443

[41]Toyoshima R, Yoshida M, Monya Y, Kousa Y, Suzuki K, Abe H, Mun B S, Mase K, Amemiya K, Kondoh H. *J. Phys. Chem. C*, **2012, 116**(35):18691-18697

[42]Jung K D, Bell A T. *J. Catal.*, **2000,193**(2):207-223

[43]Yang B, Yu X, Halder A, Zhang X B, Zhou X, Mannie G J A, Tyo E, Pellin M J, Seifert S, Su D S, Vajda S. *ACS Sustainable Chem. Eng.*, **2019,7**(17):14435-14442

[44]Grosvenor A P, Kobe B A, Biesinger M C, McIntyre N S. *Surf. Interface Anal.*, **2004,36**(12):1564-1574

[45]Sun K, Wilson A R, Thompson S T, Lamb H H. *ACS Catal.*, **2015,5** (3):1939-1948

[46]Fan Q N, He S, Hao L, Liu X, Zhu Y, Xu S L, Zhang F Z. *Sci. Rep.*, **2017,7**(1):42172

[47]d′Alnoncourt R N, Friedrich M, Kunkes E, Rosenthal D, Girgsdies F, Zhang B S, Shao L D, Schuster M, Behrens M, Schlögl R. *J. Catal.*, **2014,317**:220-228

[48]Jacobs G, Davis B H. *Appl. Catal. A*, **2005,284**(1/2):31-38

[49]Chen C S, Wu J H, Lai T W. *J. Phys. Chem. C*, **2010,114**(35):15021-15028

[50]Park J N, Mcfarland E W. *J. Catal.*, **2009,266**(1):92-97